ACS APPLIED MATERIALS & INTERFACES

www.acsami.org

Research Article

Injectable Tripeptide/Polymer Nanoparticles Supramolecular Hydrogel: A Candidate for the Treatment of Inflammatory Pathologies

Miryam Criado-Gonzalez,*[,‖] Eva Espinosa-Cano,[‖] Luis Rojo, Fouzia Boulmedais, María Rosa Aguilar, and Rebeca Hernández

Cite This: *ACS Appl. Mater. Interfaces* 2022, 14, 10068−10080

Read Online

ACCESS | Metrics & More | Article Recommendations | Supporting Information

ABSTRACT: Supramolecular peptide-based hydrogels attract great attention in several fields, i.e., biomedicine, catalysis, energy, and materials chemistry, due to the noncovalent nature of the self-assembly and functional tunable properties defined by the amino acid sequence. In this work, we developed an injectable hybrid supramolecular hydrogel whose formation was triggered by electrostatic interactions between a phosphorylated tripeptide, Fmoc-FFpY (F: phenylalanine, pY: phosphorylated tyrosine), and cationic polymer nanoparticles made of vinylimidazole and ketoprofen (poly(HKT-*co*-VI) NPs). Hydrogel formation was assessed through inverted tube tests, and its fibrillary structure, around polymer NPs, was observed by transmission electron microscopy. Interestingly, peptide self-assembly yields the formation of nontwisted and twisted fibers, which could be attributed to β-sheets and α-helix structures, respectively, as characterized by circular dichroism and infrared spectroscopies. An increase of the elastic modulus of the Fmoc-FFpY/polymer NPs hybrid hydrogels was observed with peptide concentration as well as its injectability property, due to its shear thinning behavior and self-healing ability. After checking their stability under physiological conditions, the cytotoxicity properties of these hybrid hydrogels were evaluated in contact with human dermal fibroblasts (FBH) and murine macrophages (RAW 264.7). Finally, the Fmoc-FFpY/polymer NPs hybrid hydrogels exhibited a great nitric oxide reduction (~67%) up to basal values of pro-inflammatory RAW 264.7 cells, thus confirming their excellent anti-inflammatory properties for the treatment of localized inflammatory pathologies.

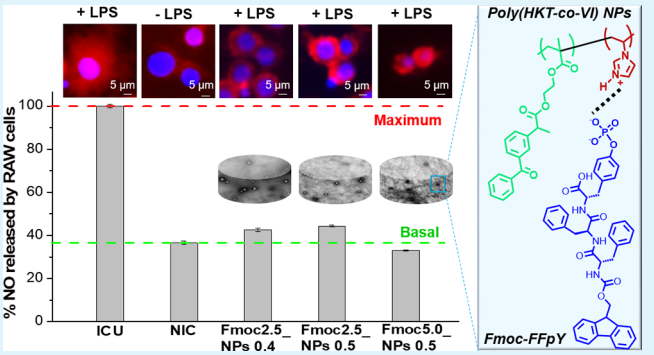

KEYWORDS: *peptides, supramolecular electrostatic self-assembly, injectable hydrogels, anti-inflammatory nanoparticles, Fmoc-FF*

1. INTRODUCTION

Supramolecular hydrogels attract great attention in several fields such as biomedicine, catalysis, energy, and materials chemistry due to the noncovalent nature of self-assembly, which makes them ideal candidates for 3D printing processing and development of injectable materials.[1−3] In this line, directed molecular self-assembly of peptides, endowed with functional tunable properties defined by the amino acids that form the peptide sequence,[4−6] at the interface of nanostructures, i.e., nanoparticles and nanotubes, has attracted widespread interest for the fabrication of magneto-responsive hydrogels,[7,8] antimicrobial coatings,[9] electronic sensors,[10] or trapping networks for water treatment,[11] among others.

Inflammatory diseases are characterized by inflammation of affected areas,[12,13] which can result in delayed healing, increased scarring, necrosis, and/or even cancer development.[12,14,15] Therefore, the inflammatory response, characterized by high quantities of pro-inflammatory macrophages, needs to be shortened to effectively improve the chronic wound healing process.[14,16] There exist several drugs, biomedical platforms, and medical therapies that can be employed to address anti-inflammatory processes.[16] In this regard, polymer nanoparticles (NPs) loaded with anti-inflammatory drugs have been widely employed. This is the case of nanoparticles made of naproxen (NAP) and dexamethasone (Dx), which have a synergistic effect on the repression of *Il12b* transcript levels, the gene that codifies *IL12-p40* in macrophages.[17] Besides, nonsteroidal anti-inflammatory drugs (NSAIDs) such as ketoprofen (HKT) have also been combined with Dx leading to anti-inflammatory NPs.[18] However, governed by their cellular internalization, the

Received: November 26, 2021
Accepted: February 9, 2022
Published: February 18, 2022

anti-inflammatory effect of NPs is limited by the quantity taken up by cells and difficult to control by targeting inflamed areas without affecting healthy tissues.[19]

These problems can be solved by embedding NPs in a self-healing hydrogel matrix, which can be injected into the target areas for treatment. *N*-Fluorenyl-9-methoxycarbonyl (Fmoc) bearing peptides, mainly assembled by $\pi-\pi$ stacking of the aromatic Fmoc units leading to β-sheets and α-helix conformations,[20,21] have shown intrinsic anti-inflammatory properties.[22,23] However, β-sheet-rich supramolecular assemblies are associated with various amyloid degenerative disorders, e.g., type 2 diabetes, Alzheimer's, and Parkinson's diseases, which makes it necessary to regulate this structural arrangement to form helix or random coil conformations during the self-assembly.[24,25] Among different self-assembling peptides, Fmoc-FF has been widely used to fabricate supramolecular hydrogels through solubilization in NaOH or DMSO solvents, and subsequent gelation through pH or temperature triggers.[26,27] As previously reported,[28] the presence of organic solvents can be avoided by the incorporation of tyrosine phosphate in the amino acid sequence leading to a water-soluble peptide, Fmoc-FFpY. Then, Fmoc-FFpY peptide can be self-assembled by enzymatic dephosphorylation in the presence of alkaline phosphatase (AP) forming supramolecular hydrogels (Fmoc-FFY),[28,29] with good biocompatibility, cell adhesion,[30] and antimicrobial properties.[9] However, their very low elastic modulus makes them difficult to handle. This problem can be overcome by assembling this peptide through electrostatic interactions with amine-charged polymers such as poly(allylamine hydrochloride) (PAH) in solution.[31] The main drawback of these systems is the limited biocompatibility of PAH, reducing the applicability of these hydrogels for biomedical applications. Therefore, herein, we present the development of a self-healing supramolecular hydrogel formed by electrostatic interaction of the phosphorylated peptide, Fmoc-FFpY, at the interface of fully biocompatible cationic polymer nanoparticles, made of vinylimidazole and ketoprofen (poly(HKT-*co*-VI) NPs). The electrostatic interaction between both components allowed us to minimize the β-sheet conformation, being the α-helix arrangements the prominent ones as revealed by circular dichroism measurements. In addition, the hydrogels showed anti-inflammatory properties, from the contact of immune RAW macrophages cells with the interface of the nanoparticles, together with a shear thinning behavior and self-healing properties to be able to be injected into target areas, which make them ideal candidates for the treatment of inflammatory pathologies.

2. EXPERIMENTAL SECTION

2.1. Materials. Fmoc-FFpY was provided by Pepmic (Suzhou, China). Sodium tetraborate anhydrous (borax), phosphate-buffered saline at pH 7.4 (PBS), and Dulbecco's modified Eagle's medium and additives, trypsin, glutaraldehyde, MTT (thiazolyl blue formazan), Tween 20, lipopolysaccharide (LPS), and Griess reagent (modified) were purchased from Sigma-Aldrich. Fetal bovine serum (FBS) was provided by Gibco. All reactants were used as received. Poly(HKT-*co*-VI) nanoparticles employed for the hydrogel formation were fabricated following a protocol previously reported by Espinosa-Cano et al.[18] Briefly, poly(HKT-*co*-VI) nanoparticles were obtained through nanoprecipitation by adding dropwise an organic solution of the copolymer, poly(HKT-*co*-VI) (10 mg mL^{-1} in acetone/ethanol (80:20)) to an aqueous buffer solution (0.1 M acetic acid and 0.1 M NaCl at pH 4). Then, the remaining organic solvent was evaporated, leading to the final dispersion of nanoparticles, with a concentration of 1 mg mL^{-1} and an average hydrodynamic diameter of ~120 nm, which was stored at 4 °C for further experiments.

2.2. Hydrogel Formation. Hydrogels were formed by mixing Fmoc-FFpY solutions (in 25 mM borax buffer at pH 9.5) with a poly(HKT-*co*-VI) nanoparticles dispersion at different ratios. Three different hydrogels were obtained with final concentrations of 5 mg mL^{-1} Fmoc-FFpY/0.5 mg mL^{-1} NPs, 2.5 mg mL^{-1} Fmoc-FFpY/0.5 mg mL^{-1} NPs, and 2.5 mg mL^{-1} Fmoc-FFpY/0.4 mg mL^{-1} NPs, named Fmoc5_NPs0.5, Fmoc2.5_NPs0.5, and Fmoc2.5_NPs0.4, respectively. The final hydrogel volume was 400 μL for the inverted tube and rheological tests and 500 μL for the cell culture. The fibrillary gel network was obtained by placing the nanoparticles dispersion in contact with the peptide solution for 24 h to guarantee that a steady state in the gel formation was achieved. The pH of the hydrogel is 5.

2.3. ζ-Potential. ζ-Potential of nanoparticles dispersion and hydrogels was measured by laser Doppler electrophoresis (LDE) using a Malvern Nanosizer NanoZS instrument equipped with a 4 mW He−Ne laser (λ = 633 nm) at a scattering angle of 173° and at 25 °C. Three measurements of 20 runs were performed for each sample.

2.4. Transmission Electron Microscopy (TEM). The morphology of the hydrogels was observed by TEM and cryo-TEM. Images were taken at 100 000 V and a magnification of 10 000 in a JEOL JEM-1230 electron microscope equipped with a digital camera CMOS TVIPS Tem-Cam 16 megapixel and a cryo-holder. TEM samples were observed under negative staining by incubating the Fmoc-FFpY/NPs hydrogels with a heavy-metal salt solution, formed by 1% uranyl acetate and 1% phosphotungstic acid, for 5 min, followed by 2 min washing. Cryo-TEM samples were prepared by placing 4 μL of each Fmoc-FFpY/NPs hydrogel on a carbon-coated copper grid to be subsequently frozen cryogenically in a Cryoplunge (GATAN) adapted with a Vitrorobot (FEI).

2.5. Fluorescence Spectroscopy. It was performed in a PerkinElmer LS 55 fluorescence spectrometer at 25 °C. All fluorescence spectra were recorded between 300 and 420 nm at an excitation wavelength of 290 nm by placing the sample between two quartz slides, leading to a path length of about 0.1 mm.

2.6. Fourier Transform Infrared (FTIR) Spectroscopy. Spectra were recorded between 850 and 1720 nm in the attenuated total reflectance (ATR) mode using a PerkinElmer Spectrum Two FT-IR Spectrometer. Measurements were performed at 25 °C after drying the hydrogels at room temperature to remove water.

2.7. Circular Dichroism (CD). Spectra were recorded between 190 and 320 nm using a Jasco J-815 spectropolarimeter with a wavelength data pitch of 0.2 nm. Measurements were performed at 25 °C using quartz slides of 1 mm thickness. Samples were placed between the two slides leading to a path length of about 0.1 mm.

2.8. Rheological Characterization. Rheological properties were measured using an AR-G2 rheometer (TA Instruments) with a cross-hatched plate geometry of 20 mm diameter and 1 mm gap. Strain measurements were carried out from 0.01 to 1000% at 1 Hz and 37 °C. Frequency sweeps were performed from 10 to 0.01 Hz at 1% strain and 37 °C. The shear thinning behavior was evaluated by measuring the share viscosity in continuous flow at share rates from 0.01 to 1000 s^{-1} at 37 °C. To demonstrate the self-recovery properties, G' and G'' were evaluated using the dynamic step strain amplitude test by varying the strain between 1 and 1000% at 25 and 37 °C.

2.9. Hydrogels Stability under Physiological Conditions and Delivery Assays. Hydrogels were incubated with 1 mL of phosphate-buffered saline (PBS) at 37 °C. After different time intervals, 1, 2, 3, 7, 14, and 21 days, the supernatant was removed and replaced with 1 mL of fresh PBS. The amounts of Fmoc-FFpY and poly(HKT-*co*-VI) NPs released at each time were evaluated by measuring the absorbance at 300 and 258 nm, respectively, using a UV−vis spectrophotometer (NanoDrop One/Onec, Thermo Scientific). The cumulative amount of each component was determined from the standard calibration curves of Fmoc-FFpY and poly(HKT-

https://doi.org/10.1021/acsami.1c22993
ACS Appl. Mater. Interfaces 2022, 14, 10068−10080

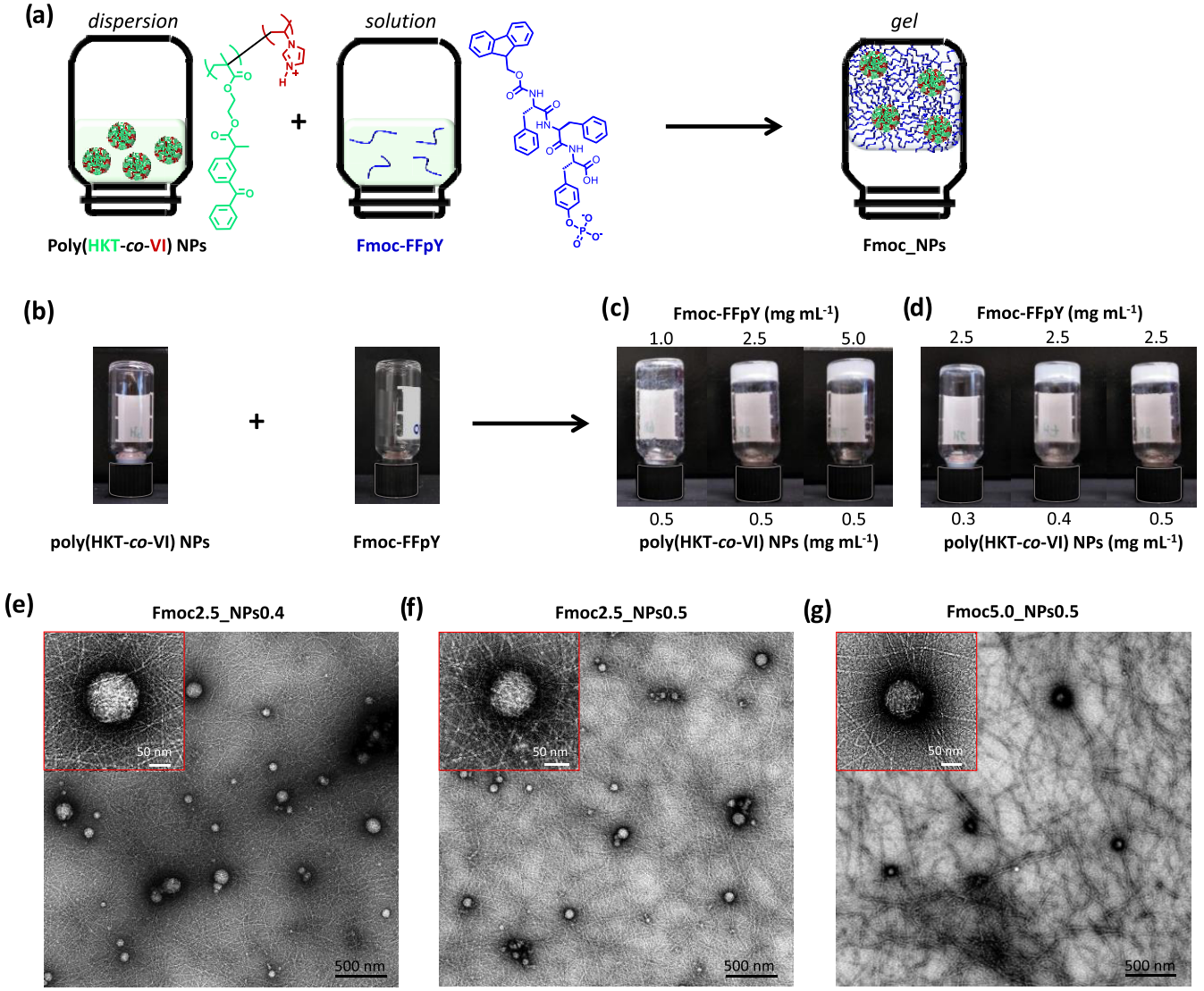

Figure 1. (a) Representative scheme of electrostatic interaction between poly(HKT-*co*-VI) NPs and Fmoc-FFpY, leading to the formation of a Fmoc_NPs hybrid hydrogel by mixing accurate proportions of poly(HKT-*co*-VI) NPs dispersion and Fmoc-FFpY solution. Inverted tube tests of the precursor poly(HKT-*co*-VI) NPs dispersion and Fmoc-FFpY solution (b) used to form supramolecular Fmoc-FFpY/poly(HKT-*co*-VI) NPs hydrogels after 24 h at (c) different Fmoc-FFpY concentrations and a fixed NPs concentration and (d) different NPs concentrations and a fixed Fmoc-FFpY concentration. The vial caps have been marked with gray contours. TEM micrographs of negatively stained Fmoc-FFpY/poly(HKT-*co*-VI) NPs hydrogels with different concentrations: (e) Fmoc2.5_NPs0.4, (f) Fmoc2.5_NPs0.5, and (g) Fmoc5_NPs0.5. Insets show the zoom-in of the peptide fibers around one single nanoparticle.

co-VI) NPs in PBS measured separately. Results are shown as mean ± standard deviation of three measurements.

2.10. Cell Culture. In vitro cell tests were performed with two different cell lines, human dermal fibroblasts (FBH) and RAW 264.7 murine macrophages (RAW) cells, at 37 °C, 5% CO_2, and 90% relative humidity. FBH cells were cultured in Dulbecco's modified Eagle's medium, enriched with 4500 mg mL^{-1} glucose (DMEM; Sigma, Saint Louis, MO) supplemented with 10% v/v fetal bovine serum (FBS; Gibco, BRL), 2% v/v L-glutamine (Sigma, Saint Louis, MO), 100 units mL^{-1} penicillin, and 100 mg mL^{-1} streptomycin, modified with 4-(2-hydroxyethyl)-1-piperazineethanesulfonic acid (HEPES). RAW cells were cultured in high-glucose DMEM (Sigma, Saint Louis, MO) supplemented with 10% v/v FBS, 2% v/v L-glutamine, and 1% v/v penicillin-G.

2.11. Cytotoxicity Assay by MTT Indirect Test. First, gels were incubated with 1 mL of FBH or RAW cell culture medium at 37 °C. At predetermined intervals, 1, 2, 3, 7, 14, and 21 days, the supernatant was removed under sterile conditions and replaced with 1 mL of fresh cell culture medium. Separately, FBH or RAW cells were seeded at densities of 9×10^4 and 1×10^5 cells mL^{-1}, respectively, in complete medium in sterile 96-well plates and incubated up to confluence. After 24 h incubation, the medium was replaced with the corresponding extracts (dilution 1:2 in complete medium) and incubated at 37 °C in humidified air with 5% CO_2 for 24 h. In the case of lipopolysaccharide-stimulated (LPS) RAW cells, 5 μL of LPS (0.5 μg mL^{-1}) was added to extracts. Afterward, cell viability was determined by AlamarBlue (Invitrogen) assay. For that purpose, the supernatant was removed and the plates were incubated with 100 μL per well of an MTT solution (10% v/v of 3-(4,5-dimethylthiazol-2-yl)-2,5-diphenyltetrazolium bromide in PBS) and incubated for 180 min at 37 °C in the dark. Then, absorbance at 570 nm was measured in a Multi-Detection Microplate Reader Synergy HT (BioTek Instruments, Winooski, VT). Results are shown as mean ± standard deviation of eight measurements and expressed as a percentage of cell viability with respect to the control (cells treated only with medium).

2.12. Cytotoxicity Assay by Live/Dead Direct Test. Gels were formed directly in 24-well plates under sterile conditions by mixing Fmoc-FFpY and poly(HKT-*co*-VI) NPs at different ratios and

https://doi.org/10.1021/acsami.1c22993
ACS Appl. Mater. Interfaces 2022, 14, 10068−10080

incubated at 37 °C for 24 h. Then, the gels were washed once with 1 mL of PBS for 5 min and twice with 1 mL of FBH or RAW cell culture medium each time. Subsequently, FBH or RAW cells were seeded at a density of 1×10^5 cells mL^{-1} on top of the gels and incubated at 37 °C in humidified air with 5% CO_2. After 24 h incubation, the medium was replaced with 1 mL of fresh cell culture medium and incubated for another 24 h under the same conditions. Subsequently, cell viability was determined using the Live/Dead viability/cytotoxicity kit (Sigma-Aldrich). The kit contains calcein-AM (4 mM in anhydrous DMSO) and ethidium homodimer-1 (2 mM in DMSO/H_2O 1:4 (v/v)), which allowed staining live cells in green and dead cells in red, respectively. For that purpose, the supernatant was removed, gels were washed with 1 mL of PBS, and a mixture of 25 μL of fresh cell culture medium without phenol red and 25 μL of the live/dead kit was added to them and incubated for 15 min at room temperature in the dark before observation by fluorescence microscopy. The stained cells were visualized with a Nikon Eclipse TE2000-S epifluorescence microscope with a 4× objective lens, and ImageJ software was used to calculate the area covered by live and dead cells. Cell viability percentage was obtained by comparison of the live cell area with respect to the death cell area of each sample. Samples were tested by duplicate, and images were taken in four different points of each sample.

2.13. Direct Cell Adhesion Assay. The morphology of the cells directly in contact with the hydrogels was visualized after a cell adhesion assay following the above-mentioned procedure, but instead of using the live/dead kit, the cells were stained according to the following protocol at the end of the cell contact assay. After washing with 1 mL of PBS, the cells were fixed/permeabilized with 3.7% w/v paraformaldehyde (PFA) in PBS for 1 h. PFA was removed, and samples were washed twice with 1 mL of PBS. After removing PBS, 200 μL of Triton 0.05% w/v in PBS was added and kept in contact for 20 min at room temperature. Later, the samples were washed twice with 1 mL of PBS and brought in contact with 100 μL of Hoechst (dilution 1:1000 from 10 mg mL^{-1} in PBS) plus 100 μL of phalloidin-rhodamine (dilution 1:100 in PBS from stock) and incubated for 40 min in the dark. Subsequently, the samples were washed once with 400 μL of PBS and then with 1 mL of Milli-Q water. After that, 200 μL of Tween 20 (0.02% v/v in PBS) was added and incubated for 5 min in the dark. Finally, the samples were washed with 1 mL of Milli-Q water and observed by fluorescence microscopy using a Nikon Eclipse TE2000-S epifluorescence microscope with a 20× objective lens. ImageJ software was used to calculate the area covered by the nucleus and cytoskeleton.[32] The cell area was calculated as the sum of the nucleus area plus the cytoskeleton area by counting at least 20 cells. The samples were tested in duplicate, and images were taken in four different points of each sample.

2.14. Nitric Oxide (NO) Assay for Anti-Inflammatory Properties. For the indirect NO assay, first, gels were incubated with 1 mL of RAW cell culture medium at 37 °C. After predetermined time intervals, 1, 2, 3, 7, 14, and 21 days, the supernatant was removed under sterile conditions and replaced with 1 mL of fresh cell culture medium. Separately, RAW cells were seeded at a density of 1×10^5 cells mL^{-1} in complete medium in a 96-well plate and incubated up to confluence. After 24 h incubation, the medium was replaced with the corresponding extracts and incubated at 37 °C in humidified air with 5% CO_2 for 24 h. In the case of lipopolysaccharide-stimulated (LPS) RAW cells, 5 μL of LPS (0.5 μg mL^{-1}) was added to extracts to simulate inflammatory conditions (ICU). Afterward, NO released by macrophages was determined using the Griess reagent-modified kit (Sigma-Aldrich) according to the manufacturer's instructions. The supernatant (75 μL) was brought in contact with 25 μL of Griess reagent and incubated for 15 min in the dark. In the case of NO direct assay, gels were formed directly in 24-well plates under sterile conditions by mixing poly(HKT-*co*-VI) NPs and Fmoc-FFpY at different ratios and incubated at 37 °C for 24 h. Then, the gels were washed once with 1 mL of PBS for 5 min and twice with 1 mL of RAW cell culture medium each time. Subsequently, RAW cells at a density of 1×10^5 cells mL^{-1} were seeded on top of the gels and incubated at 37 °C in humidified air with 5% CO_2. After 24 h incubation, the medium was replaced with 1 mL of fresh cell culture medium and 5 μL of LPS (0.5 μg mL^{-1}) was added to the LPS-stimulated RAW cells and incubated for another 24 h under the same conditions. Subsequently, NO released by macrophages was determined as previously. In both cases, results are shown as mean ± standard deviation of eight measurements and expressed as a percentage of NO released with respect to the control (LPS-activated cells treated only with medium without extracted aliquots or hydrogels).

2.15. Statistical Analysis. Statistical analyses were performed using one-way ANOVA, at a significance level of $^{**}p < 0.01$, and Tukey's multiple comparison test.

3. RESULTS AND DISCUSSION

3.1. Fmoc-FFpY/Poly(HKT-*co*-VI) NPs Hydrogel Formation and Morphological Characterization. Fmoc-FFpY peptide solution is negatively charged reaching a ζ-potential value of −36.1 ± 2.0 mV at 2.5 mg mL^{-1}, and poly(HKT-*co*-VI) NPs are positively charged with a value of +25.7 ± 0.8 mV at 0.5 mg mL^{-1}. The supramolecular hybrid hydrogels formation should be triggered by electrostatic interactions between a phosphorylated tripeptide, Fmoc-FFpY, and positively charged poly(HKT-*co*-VI) NPs (Figure 1a-b). The optimal conditions to form the hybrid hydrogel were assessed by the inverted tube test. By keeping the NPs concentration constant at 0.5 mg mL^{-1}, the hydrogel is formed above 2.5 mg mL^{-1} Fmoc-FFpY (Figure 1c). The effect of the NPs concentration was also studied by keeping the Fmoc-FFpY concentration fixed at 2.5 mg mL^{-1} (Figure 1d). A poly(HKT-*co*-VI) NPs concentration higher than 0.4 mg mL^{-1} is necessary to form the hydrogel. Under the optimal conditions, the hybrid hydrogel formation takes place in less than 15 min after mixing the NPs dispersion and the peptide solution (Figure S1 in the Supporting Information (SI)). This fast gelation is due to the electrostatic interactions settled between Fmoc-FFpY and poly(HKT-*co*-VI) NPs, the main driving force of the peptide self-assembly, as found for Fmoc-FFpY/PAH gelation.[33]

Three hybrid hydrogels were then studied and prepared at an Fmoc-FFpY concentration of 2.5 or 5 mg mL^{-1} and a poly(HKT-*co*-VI) NPs concentration of 0.4 or 0.5 mg mL^{-1}, named Fmoc2.5_NPs0.4, Fmoc2.5_NPs0.5, and Fmoc5_NPs0.5. The hydrogels morphology was visualized by TEM under negative staining, where peptide fibers are visualized in white (Figure 1e−g). Independently of the peptide or NPs concentrations, a homogeneous dispersion of poly(HKT-*co*-VI) NPs, with an average diameter of 110 ± 26 nm, is observed all over the samples. Several micrometer length fibers with entanglements between them are observed around the NPs. These fibers are characteristic of Fmoc-FFpY in the self-assembly state.[29,31] No significant differences are detected in the fibers' diameter, being ∼5.0 nm for the three samples under study. A high density of Fmoc-FFpY fibers is observed around the isolated NPs, easily visualized by zooming in these areas (Figure 1e−g, insets). In the case of the poly(HKT-*co*-VI) NPs dispersion (Figure S2a in the SI), only NPs with a diameter of 115 ± 28 nm are visualized with no fibers. The precursor Fmoc-FFpY solution showed single isolated fibers without the presence of entanglements (Figure S2b in the SI).

3.2. Secondary Structure of the Fmoc-FFpY/Poly(HKT-*co*-VI) NPs Self-Assembly. A key feature of the Fmoc-peptides self-assembly is the Fmoc moieties stacking, revealed by fluorescence spectroscopy due to the excimer formation of fluorenyl (Figure 2a). The spectrum of Fmoc-FFpY in solution

https://doi.org/10.1021/acsami.1c22993
ACS Appl. Mater. Interfaces 2022, 14, 10068−10080

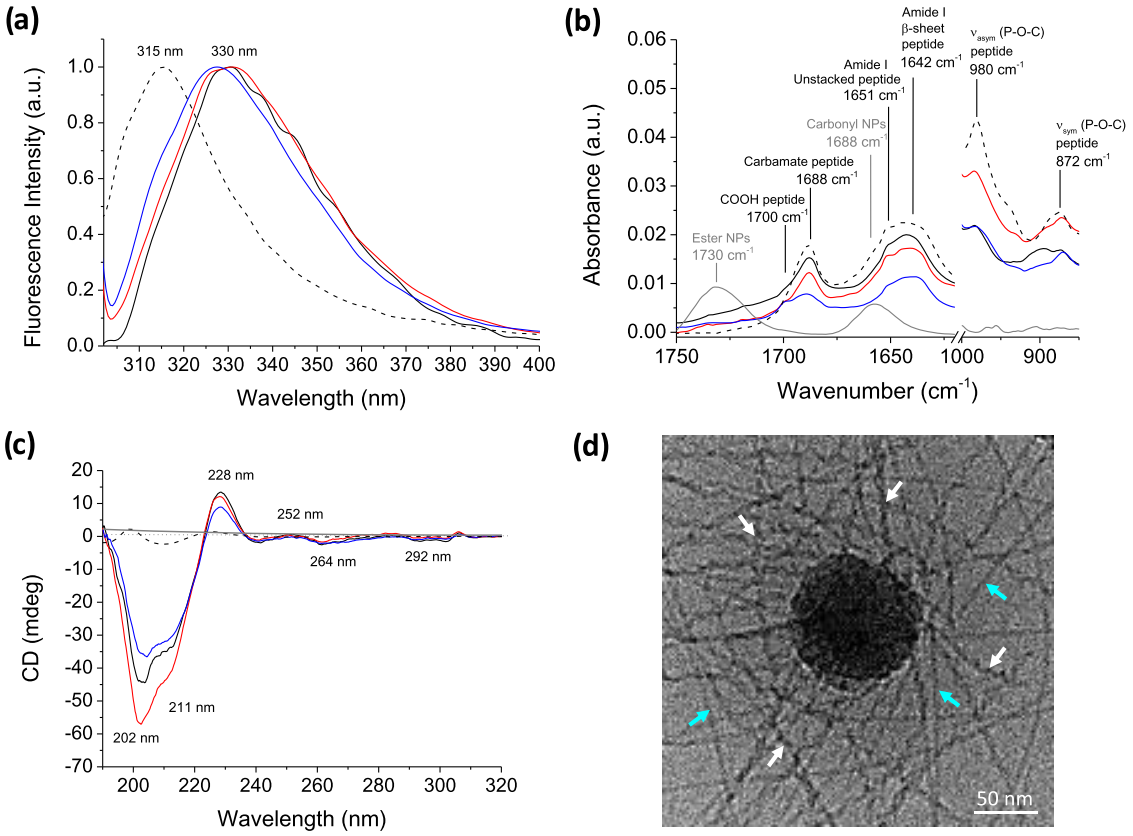

Figure 2. (a) Fluorescence spectra normalized to the peak at 315 nm. (b) ATR-FTIR and (c) CD spectra of poly(HKT-*co*-VI) NPs (solid gray curve), Fmoc-FFpY in solution (dashed black curve), Fmoc2.5_NPs0.4 (blue curve), Fmoc2.5_NPs0.5 (red curve), and Fmoc5_NPs0.5 (black curve) hybrid hydrogels. (d) Cryo-TEM micrograph of Fmoc0.5_NPs0.05 after 5 min mixing, where white and blue arrows show twisted and nontwisted fibers, respectively.

shows a band at 315 nm, which is attributed to non-self-assembled fluorenyl moieties.[34] Once the peptide is brought in contact with poly(HKT-*co*-VI) NPs, this band is shifted up to 330 nm due to the fluorenyl excimer formation after self-assembly.[35] These results are in agreement with previous works related to electrostatic self-assembly of Fmoc-FFpY in the presence of a polycation solution.[31,33] To get further insight into the self-assembly mechanism, the secondary structure resulting from the interaction of Fmoc-FFpY and poly(HKT-*co*-VI) NPs was first analyzed by ATR-FTIR spectroscopy (Figure 2b). The FTIR spectrum of poly(HKT-*co*-VI) NPs shows two peaks at 1656 and 1730 cm^{-1}, corresponding to conjugated carbonyl C═O of ketoprofen[36] and ester bonds.[37] The peptide Fmoc-FFpY presents the carbamate peak at 1688 cm^{-1},[38] the amide I band with two peaks at 1651 and 1642 cm^{-1}, corresponding to unstacked peptide and β-sheets structures,[39] and phosphate peaks at 980 and 872 cm^{-1}.[40] The Fmoc-FFpY/poly(HKT-*co*-VI) NPs hybrid hydrogel spectra have the peaks of both compounds, with a β-sheet peak at 1642 cm^{-1} and the apparition of COOH peak at 1700 cm^{-1} attributed to the C-terminal carboxylic group of Fmoc-FFpY.[41] The peptide seems to be in its protonated form. The presence of the phosphate peaks indicates that the peptide is not dephosphorylated. As the poly(HKT-*co*-VI) NPs have a peak at 1656 cm^{-1}, it appears difficult to decompose the amide I band of the Fmoc-FFpY/poly(HKT-*co*-VI) NPs hydrogel to determine the contribution of each secondary conformation to the peptide assembly.

Then, we characterized the structural arrangement by CD (Figure 2c). The spectrum of the precursor Fmoc-FFpY in solution shows a positive peak at 199 nm together with a negative band at 210 nm, characteristics of β-sheet conformation. When the peptide solution is brought in contact with poly(HKT-*co*-VI) NPs, a positive peak is observed at 190 nm together with two strong negative peaks at 202 and 211 nm, which is the α-helix conformation signature, suggesting a structural transition from β-sheets to α-helix arrangements.[25,42] Fmoc-FFpY/poly(HKT-*co*-VI) NPs spectra also present two negative bands at 264 and 292 nm, assigned to offset face-to-face stacking of the Fmoc moieties and the fluorenyl absorption, respectively.[43] Moreover, the two positive peaks located at 228 and 252 nm are the signature of stacking interactions of the aromatic units of Fmoc-FFpY.[44] Both results, from FTIR-ATR and CD experiments, indicate that the peptide self-assembly induced by electrostatic interaction with positively charged polymeric NPs is a combination of β-sheets and α-helix fiber arrangements with the main contribution of α-helix structures. The peptide self-assembly morphology was further studied in detail by cryo-TEM under diluted conditions, at 0.5 mg mL^{-1} Fmoc-FFpY and 0.05 mg mL^{-1} poly(HKT-*co*-VI) NPs (Figure 2d). Two different morphologies, nontwisted and twisted fibers, are observed, as shown for other kinds of peptides.[45] Nontwisted fibers (blue arrows) can be attributed to the β-sheet conformation, whereas twisted fibers (white arrows) can be assigned to α-helix arrangements according to the literature.[24,25] It is also possible to distinguish more twisted than nontwisted fibers, corroborating the α-helix

https://doi.org/10.1021/acsami.1c22993
ACS Appl. Mater. Interfaces 2022, 14, 10068−10080

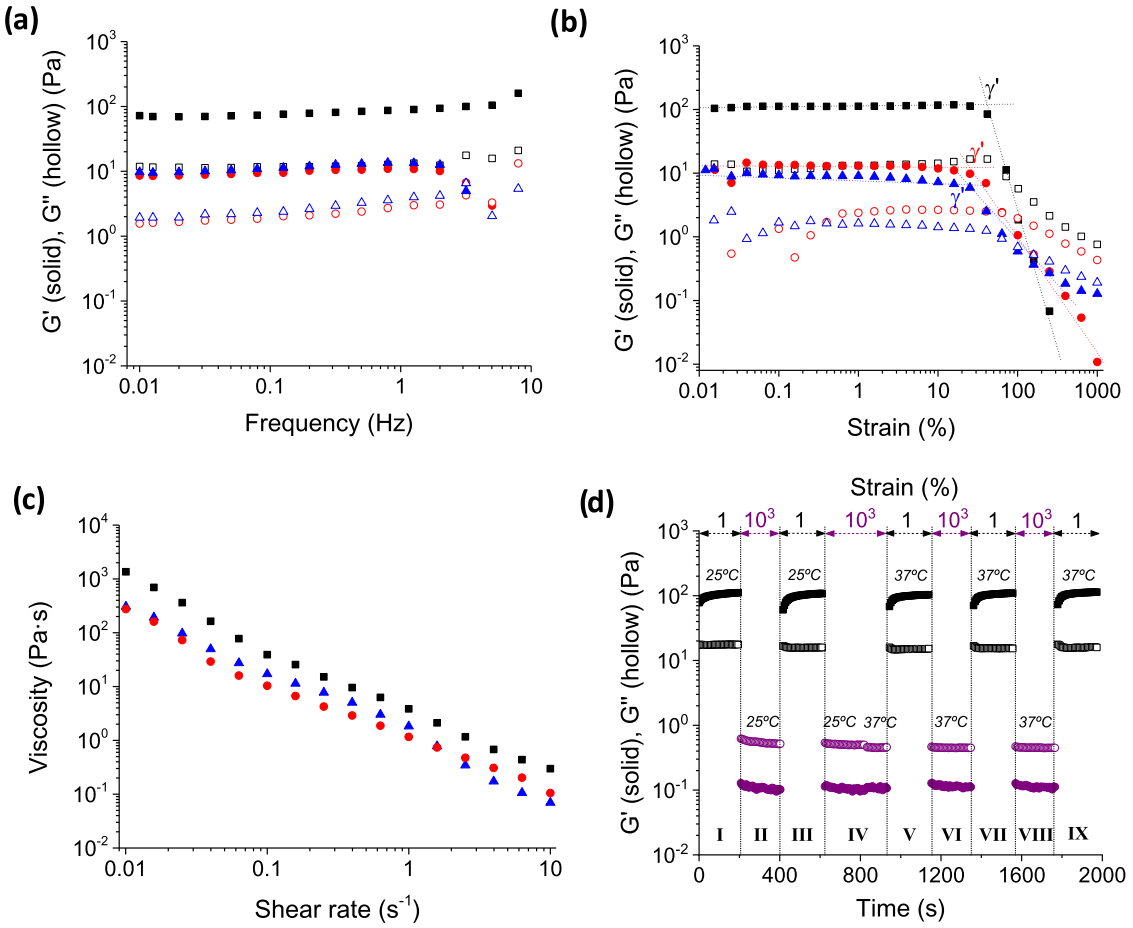

Figure 3. Rheological properties of Fmoc-FFpY/poly(HKT-*co*-VI) NPs hydrogels prepared at different concentrations, Fmoc2.5_NPs0.4 (▲), Fmoc2.5_NPs0.5 (●), and Fmoc5_NPs0.5 (■). Storage modulus (G'—solid symbols) and loss modulus (G''—hollow symbols) as a function of (a) frequency (0.01−10 Hz, 1% strain) and (b) strain (0.01−1000%, 1 Hz) at 37 °C. Shear viscosity as a function of the applied share rate at 37 °C (c). Dynamic step strain amplitude test (1 or 1000% strain) of the hydrogel Fmoc5_NPs0.5 to mimic the injectability conditions (d) at 25 and 37 °C.

structures of the hydrogel observed by CD. Another feature related to the α-helix structures is the smaller diameter of the fibers, which are 5 nm, compared to the fiber diameter of the β-sheets structures of the same peptide when self-assembled by enzymatic dephosphorylation, reported at 10 nm.[29,31] This finding has been also reported when Fmoc-FF is self-assembled in the presence of 4,4-bipyridine[24] and Na^+ or Zn^+ cations.[25]

3.3. Determination of the Rheological Properties and Stability of Fmoc-FFpY/Poly(HKT-*co*-VI) NPs Hydrogels under Simulated Physiological Conditions. Recently, a lot of research efforts have been aimed at designing and developing hydrogels with self-healing and injectability properties toward less invasive delivery agents of therapeutics.[46] The key factors of an injectable hydrogel are to have appropriate mechanical properties, stability under physiological conditions, and shear thinning behavior with a fast phase transition between liquid- and solid-like states.[47] Oscillatory frequency sweep tests corroborate the gel formation for peptide concentrations above 2.5 mg mL^{-1} and NPs concentrations above 0.4 mg mL^{-1} as the elastic modulus (G') and the loss modulus (G'') are independent of the frequency and G' is higher than G'' over the tested frequency range (Figure 3a). Fmoc2.5_NPs0.4 and Fmoc2.5_NPs0.5 hydrogels have a G' (G'') of the order of 10 Pa (2 Pa) at the frequency of 1 Hz (strain 0.1%). At a fixed peptide concentration of 2.5 mg mL^{-1}, NPs concentration showed no influence under the studied conditions. At a fixed 0.5 mg mL^{-1} NPs concentration, G' displays almost an 8-fold increase, from 10.8 ± 1.0 to 83.8 ± 5.2 Pa (at 1 Hz frequency, 0.01% strain), with a 2-fold increase of Fmoc-FFpY concentration from 2.5 to 5 mg mL^{-1}. An increase of the critical deformation, determined through strain sweeps, is also observed from ∼26 to ∼40% (Figure 3b). The increase of the elastic modulus and resistance to the deformation of the hybrid hydrogel with the concentration in peptides can be related to an increase in the number of fibers and entanglements between them in its structure. The elastic modulus of Fmoc2.5_NPs0.5 hybrid hydrogel is comparable to the ones of other peptide-based hydrogels like Fmoc-FF (G' ∼ 80 Pa),[48] Fmoc-GFFRGD (G' ∼ 100 Pa),[49] or peptide amphiphiles (PA), including PA-RGDS and PA-VAPG, with G' around 100 Pa.[50]

One requirement of injectable materials is to exhibit shear thinning properties. For such purpose, the shear thinning behavior of the hybrid hydrogel was ascertained through flow tests, where a drastic viscosity decrease with shear rate is observed in all cases (Figure 3c). At the same time, self-healing hydrogels need to present tixotropic properties, that is, recovery of their viscoelastic properties after being subjected to a shear force.[1] To test that, dynamic step strain amplitude tests were performed on the Fmoc5_NPs0.5 hydrogel by

https://doi.org/10.1021/acsami.1c22993
ACS Appl. Mater. Interfaces 2022, 14, 10068−10080

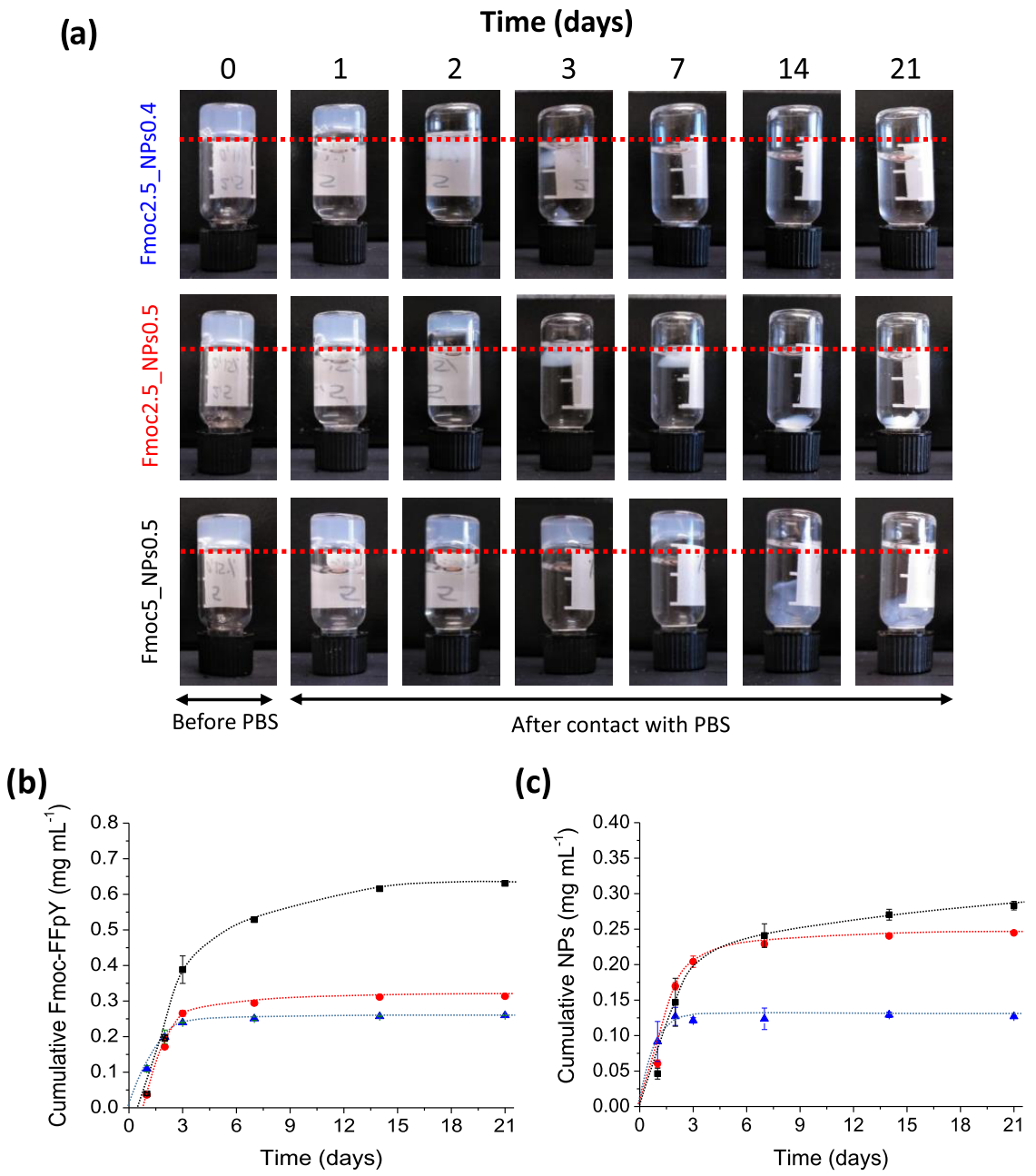

Figure 4. (a) Photographs corresponding to inverted tube tests of Fmoc-FFpY/poly(HKT-*co*-VI) NPs hydrogels with different concentrations before (time 0) and after contact with PBS over 21 days. Dashed lines are a guide to the eye. Cumulative release of (b) Fmoc-FFpY and (c) poly(HKT-*co*-VI) NPs from Fmoc2.5_NPs0.4 (▲), Fmoc2.5_NPs0.5 (●), and Fmoc5_NPs0.5 (■) hydrogels over time. Dashed lines are a guide to the eye.

varying the strains between 1 and 1000% at short times, 200 s, and the temperature between 25 °C (room temperature) and 37 °C (physiological temperature) (Figure 3d).

At stage I of Figure 3d (γ = 1%, T = 25 °C), the Fmoc5_NPs0.5 hydrogel shows a solidlike behavior ($G' > G''$). After increasing the strain up to 1000% (stage II), G' drastically decreases and a liquid-like state is reached ($G'' > G'$). A total recovery of the initial mechanical properties is observed when the gel is brought to stage III (γ = 1%, T = 25 °C), as G' increases quickly exhibiting a solid-like behavior again ($G' > G''$). Then, the hydrogel was subjected to high strain (stage IV, γ = 1000%, T = 25 °C), and the sample changes to a liquid-like state, which is maintained after increasing the temperature to 37 °C. Subsequent dynamic strain steps were performed at 37 °C (stages V to IX) showing a complete elastic modulus recovery of the hydrogel after several solid−liquid phase changes, which proves the excellent properties of this supramolecular hybrid hydrogel as a potential injectable candidate. In the case of both hydrogels formed with a lower Fmoc-FFpY concentration, i.e., Fmoc2.5_NPs0.4 and Fmoc2.5_NPs0.5, solid−liquid phase transitions were also observed after several strain variations, but the initial mechanical properties (G') were not fully recovered (Figure S3 in the SI).

Before the biological tests, the stability of Fmoc-FFpY/poly(HKT-*co*-VI) NPs hydrogels under simulated physiological conditions was evaluated by the inverted tube test up to 21 days by bringing the hydrogels in contact with phosphate-

https://doi.org/10.1021/acsami.1c22993
ACS Appl. Mater. Interfaces 2022, 14, 10068−10080

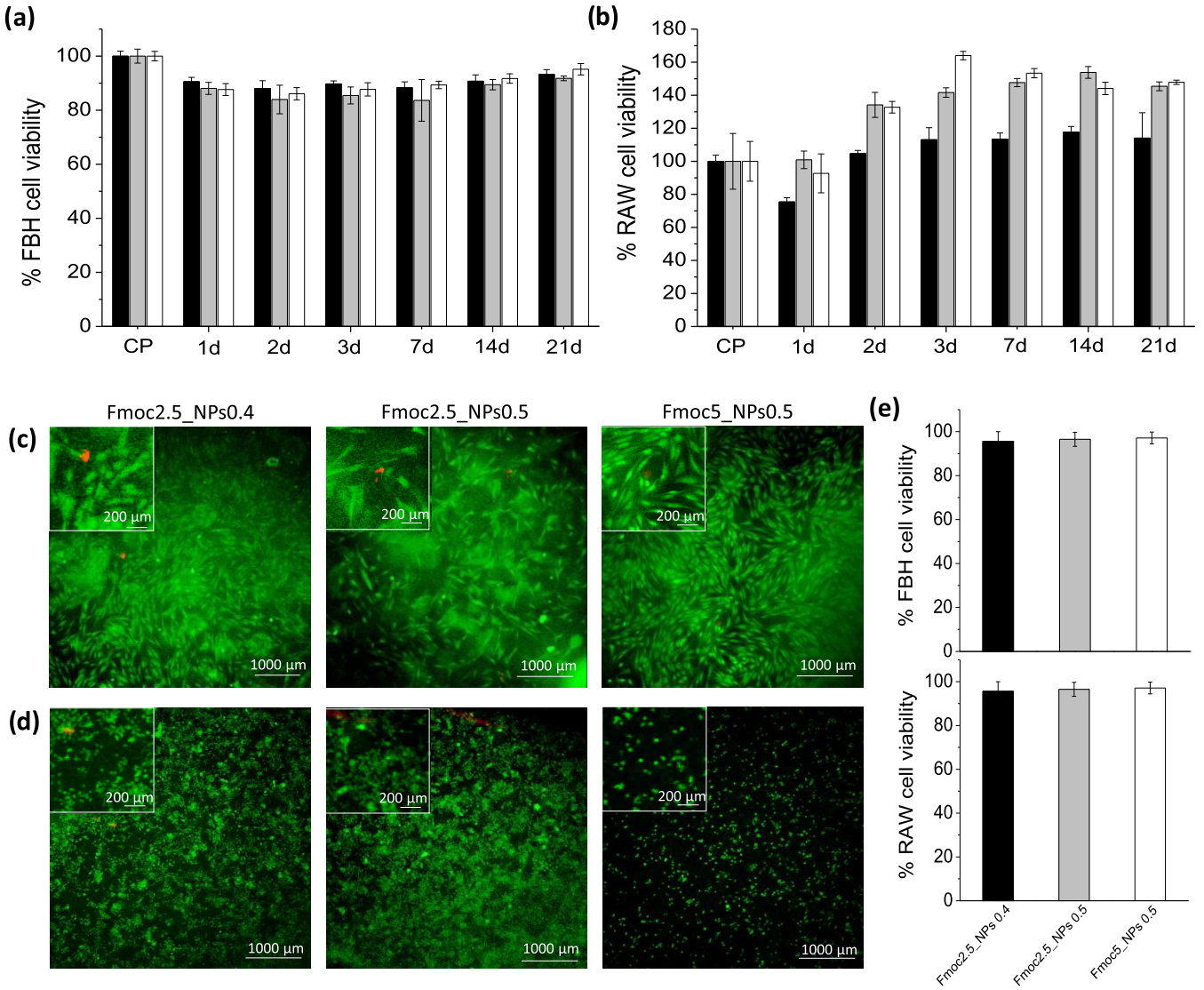

Figure 5. Fmoc-FFpY/poly(HKT-*co*-VI) NPs hydrogels cytotoxicity, Fmoc-FFpY2.5_NPs0.4 (black), Fmoc2.5_NPs0.5 (gray), and Fmoc5_NPs0.5 (white). MTT indirect tests of (a) FBH and (b) RAW cells seeded with aliquots withdrawn from the cell culture medium in contact with the hydrogels (mean and standard deviation from $n = 2$) and fluorescence microscopy images of the live/dead direct assay of (c) FBH and (d) RAW cells seeded on the surface of the hydrogels for 48 h. The insets show specific areas with dead cells (red staining). (e) Cell viability obtained by calculating the ratio of total live/total cells (live and dead) using ImageJ software (mean and standard deviation from $n = 2$).

buffered saline (PBS) at 37 °C (Figure 4). Fmoc2.5_NPs0.4 and Fmoc2.5_NPs0.5 hydrogels decrease in size and float in the supernatant after 2 and 3 days in PBS, respectively. The hydrogel formed with a higher Fmoc-FFpY concentration, Fmoc5_NPs0.5, showed better stability in PBS, keeping its consistency up to 7 days. The presence of a higher number of fibers and entanglements in the gel network could explain the prolonged stability at higher concentrations in peptides. Thus, the amount of Fmoc-FFpY and poly(HKT-*co*-VI) NPs released were measured over 21 days by UV−vis spectroscopy at wavelengths of 300 and 254 nm, respectively (Figure 4b,c). In the case of Fmoc2.5_NPs0.4 and Fmoc2.5_NPs0.5 hydrogels, a fast release of Fmoc-FFpY is observed up to 3 days and then reaches a plateau (Figure 4b), which is consistent with the inverted tube test results (Figure 4a). In the case of Fmoc5_NPs0.5, the release is fast for 3 days and slows down to reach a plateau after 14 days, thus confirming improved stability of the gel.

Regarding the release of polymer NPs, a fast release from the hydrogels is obtained over 2−3 days followed by a plateau for the Fmoc2.5_NPs0.4 hydrogel and a slowing down for Fmoc2.5_NPs0.5 after 7 days. On the contrary, in the case of Fmoc5_NPs0.5, a more sustained release of NPs is observed. In this case, the release profiles of both components follow the same tendency with a fast release for 2 days, of 4 μg mL^{-1} h^{-1} in peptide and 3 μg mL^{-1} h^{-1} in NPs, reaching a plateau after 14 days. In a final solution at pH 5 of 0.05 M acetic buffer/0.05 M NaCl, the electrostatic interactions between Fmoc-FFpY and poly(HKT-*co*-VI) NPs are probably gradually disassembled in PBS by the change in both pH and salt concentration, leading to the subsequent delivery of both precursors. In all cases, almost 50% of the self-assembled Fmoc-FFpY and 50% of NPs are released from the hydrogels.

Fmoc-FFpY/poly(allylamine) hydrogels, obtained by the electrostatic interaction between both components, were degraded upon contact with phosphatase with a decrease of their mechanical property due to the dephosphorylation of

https://doi.org/10.1021/acsami.1c22993
ACS Appl. Mater. Interfaces 2022, 14, 10068−10080

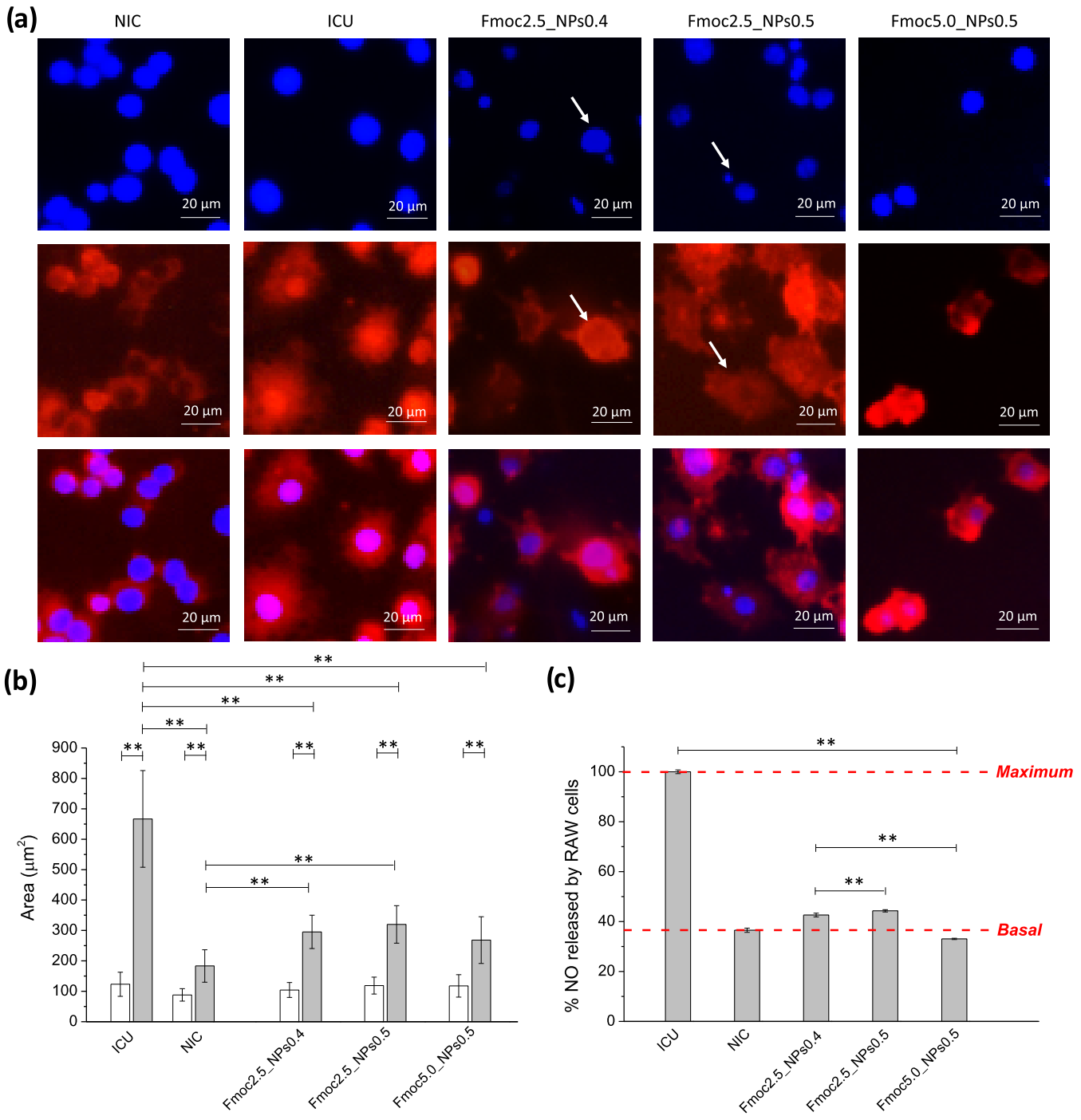

Figure 6. Anti-inflammatory properties of Fmoc-FFpY/poly(HKT-*co*-VI) NPs hydrogels toward RAW macrophages with LPS-RAW cells seeded on the plate (ICU), Non-LPS-RAW cells (NIC), and LPS-RAW cells seeded on the hydrogels. (a) Fluorescence microscopy images show cells with nuclei stained by Hoechst (top) and cytoskeleton by phalloidin-Rho (center) and merged channels (bottom). White arrows mark some multinucleated cells. (b) Nuclei (white) and total area of cells (gray) measured on 20 RAW cells with ImageJ software. (c) Nitric oxide released as mean and standard deviation (n = 6) with ANOVA results at a significance level of $^{**}p < 0.01$.

Fmoc-FFpY by the enzyme leading to the formation of Fmoc-FFY hydrogel.[31] We investigated the hydrogel stability for 48 h in contact with each culture media in the absence and in the presence of both studied cell lines (human dermal fibroblasts (FBH) and macrophages (RAW)) (Figures S4 and S5). In the absence of cells, the inverted tube tests show that Fmoc5_NPs0.5 remains stable in contact with the culture media (Figure S5a). In the presence of cells in the 24-well plate, the appearance of the hydrogel remained unaffected visually (Figure S5b). Regarding Fmoc2.5_NPs0.4 and Fmoc2.5_NPs 0.5 hydrogels, their size decreased and they were floating in the culture media without cells (Figure S4a). In the presence of cells, the hydrogel is still visible but with some cracks (Figure S5b). These results could be indicative of the relative hydrogel stability in contact with proteases and phosphatases of the cells.

3.4. Cytotoxicity Assays and Cell Viability. First of all, the cytotoxicity of Fmoc-FFpY/poly(HKT-*co*-VI) NPs hydro-

https://doi.org/10.1021/acsami.1c22993
ACS Appl. Mater. Interfaces 2022, 14, 10068−10080

gels was evaluated by the MTT indirect test. To that aim, hydrogels were brought in contact with cell culture media and supernatant aliquots were taken at different times, up to 21 days, to be subsequently put in contact with human fibroblasts (FBH) and murine macrophage (RAW) cells. After 24 h incubation with aliquots from hydrogels, the MTT test of FBH and RAW cells was performed (Figure 5a,b). In comparison to the control plate (CP), i.e., cells in cell culture media, no significant decrease of FBH cell viability is observed with FBH cell viability higher than 85% for hybrid hydrogels up to 21 days (Figure 5a). To know if Fmoc-FFpY could have an impact on FBH cell viability, a control experiment was carried out by incubating FBH cells with different concentrations of Fmoc-FFpY solutions prepared in cell culture medium (Figure S6a in the SI). The presence of Fmoc-FFpY has no cytotoxicity effect up to 0.5 mg mL^{-1} after 24 h of incubation. In the case of RAW cells in contact with the aliquots, cell viability slightly decreases on day 1 followed by a nonexpected cell proliferation over time up to 21 days, being much higher in the case of Fmoc2.5_NPs0.4 and Fmoc-FF2.5_NPs0.5 (Figure 5b). Taking into account that poly(HKT-*co*-VI) NPs do not have any potential effect on RAW cell proliferation,[18] the Fmoc-FFpY effect on RAW cell proliferation was tested by incubating the cells with different concentrations of Fmoc-FFpY solution in cell culture medium for 24 h (Figure S6b in the SI).

Interestingly, RAW cell proliferation is observed, which increases with Fmoc-FFpY concentration up to 0.25 mg mL^{-1} and decreases above this value. These results can be compared with the Fmoc-FFpY release from the hybrid hydrogel (Figure 4b). Fmoc2.5_NPs0.5 and Fmoc2.5_NPs0.4 hydrogels release close to 0.3 mg mL^{-1} Fmoc-FFpY in PBS on the second day (Figure 4b) with RAW cell proliferation values greater than or equal to 140%. Fmoc5_NPs0.5 hydrogels released 0.6 mg mL^{-1} Fmoc-FFpY in PBS after 21 days leading to limited RAW cell proliferation (less than 120%) (Figure 5b). Therefore, Fmoc-FFpY/poly(HKT-*co*-VI) NPs hydrogels are not cytotoxic and induce cell proliferation of RAW macrophages.

In a second experiment, cell viability was also analyzed by a direct assay using a live/death cell kit, which stains live cells in green and death cells in red (Figure 5c–e). In that case, the viability of FBH and RAW cells, seeded directly on the surface of Fmoc-FFpY/poly(HKT-*co*-VI) NPs hydrogels, was evaluated after 48 h contact. A high FBH cell viability is observed with most of cells alive (green staining) and only 4% of death cells (red staining) (Figure 5c). FBH cell morphology was further visualized by staining cell nuclei with Hoechst (blue staining) and cytoskeleton (F-actin fibers) with phalloidin-rhodamine (phalloidin-Rho, red staining) (Figure S7 in the SI). On Fmoc-FFpY/poly(HKT-*co*-VI) NPs hydrogels, a high cellular density of FBH is observed presenting an elongated morphology, a sign of good cell adhesion. This cellular adhesion could be influenced by the nanofibrillar structure of the hydrogels as it has been previously reported for gellan gum hydrogels showing similar morphologies to those encountered for Fmoc-FFpY/poly(HKT-*co*-VI) NPs hydrogels presented here.[51] In the case of RAW cells, a high viability is also observed with a lower RAW cell proliferation in the case of Fmoc5_NPs0.5 hydrogels (Figure 5d), in agreement with the results of the indirect tests (Figure 5b). This could be attributed to the Fmoc-FFpY concentration threshold that favors cell proliferation (0.25 mg mL^{-1}) (Figure S6b). Insets of the images show specific areas in the presence of dead cells. No direct cytotoxicity is observed with FBH and RAW viability higher than 95% after 48 h of contact (Figure 5e).

3.5. Anti-Inflammatory Properties of Fmoc-FFpY/poly(HKT-*co*-VI) NPs Hydrogels. Macrophages are innate immune cells that contribute to fighting infections, tissue repair, and maintaining tissue homeostasis. When activated by lipopolysaccharide (LPS), these cells have the ability to polarize to their pro-inflammatory phenotype (M_1) starting to overproduce nitric oxide (NO). The anti-inflammatory property of Fmoc-FFpY/poly(HKT-*co*-VI) NPs hydrogels was thus evaluated by measuring the NO production of RAW macrophages activated with LPS, named LPS-RAW cells, seeded on the surface of the hydrogels for 24 h (Figure 6). LPS-RAW cells seeded on the well plate were employed as positive control (inflammatory conditions untreated; ICU). Non-LPS-RAW cells seeded on hydrogels were used as negative control (noninflammatory conditions; NIC). It can be noticed that non-LPS-RAW cells yield similar results when seeded on the well plate or the hydrogels (data not shown). Macrophages morphology was determined by staining cell nuclei with Hoechst and cytoskeleton with phalloidin-Rho (Figures 6a and S8a in the SI). No significant differences in the nucleus area are detected between nonstimulated and LPS-RAW cells seeded on the hydrogels. However, significant differences in the total cell area are observed between LPS-RAW cells seeded on the hydrogels and the control samples (NIC and ICU). LPS-RAW cells seeded on the plate (ICU) showed a huge increase in the total cell area (~650 μm^2) in comparison to non-LPS-RAW cells seeded on the plate and on the hydrogels (NIC, ~200 μm^2). Interestingly, when seeded on Fmoc-FFpY/poly(HKT-*co*-VI) NPs hydrogels, LPS-RAW cells showed a clear reduction of the cell area (~300 μm^2) reaching values close to non-LPS-RAW cells seeded on the hydrogels (Figure S8b in the SI). This effect is due to the anti-inflammatory properties of the hybrid hydrogels. Moreover, in contact with the hybrid hydrogels, a high reduction of NO released by LPS-RAW cells is observed in comparison to the plate, reaching almost the basal value of non-LPS-RAW cells on the hydrogels (36.5 ± 0.8%, NIC) (Figure 6c). Indeed, 55–67% reduction of NO production is achieved after 24 h contact with a production of 42.6 ± 0.7, 44.3 ± 0.5, and 33.1 ± 0.3% for Fmoc2.5_NPs0.4, Fmoc2.5_NPs0.5, and Fmoc5_NPs0.5, respectively. The anti-inflammatory capacity of poly(HKT-*co*-VI) NPs has been proven previously with an ~15% reduction of NO released by LPS-RAW cells independently of the concentration.[18] The excellent reduction of NO production obtained from Fmoc-FFpY/poly(HKT-*co*-VI) NPs hydrogels is probably attributed to Fmoc-FFpY hydrogels. Thus, the anti-inflammatory properties of Fmoc-FFpY were tested in solution (Figure S9 in the SI). A reduction of NO produced by LPS-RAW cells is observed from ~10 to ~40% for 1×10^{-3} to 0.25 mg mL^{-1} Fmoc-FFpY solutions, where a threshold is reached, respectively. The production of NO decreases with the increase of Fmoc-FFpY concentration until reaching a threshold at 0.25 mg mL^{-1}. Poly(HKT-*co*-VI) NPs alone results in an ~15% reduction of NO release at a concentration of 0.125 mg mL^{-1}.[18] These results clearly indicate that the combination of the Fmoc-FFpY peptide and the poly(HKT-*co*-VI) NPs produces an enhanced additive anti-inflammatory effect toward LPS-RAW cells with respect to that exhibited by both components separately. The anti-inflammatory effect of the hybrid hydrogels is maintained with a slight decrease up to 21 days (Figure S10 in the SI), in agreement with the release

https://doi.org/10.1021/acsami.1c22993
ACS Appl. Mater. Interfaces 2022, 14, 10068–10080

profiles of Fmoc-FFpY and poly(HKT-*co*-VI) NPs (Figure 4). It is interesting to note that LPS induced the formation of some multinucleated giant cells (MGCs) on Fmoc2.5_NPs0.4 and Fmoc2.5_NPs0.5 hydrogels. Previous results have associated the presence of MNGs to a shift in macrophage polarization from M1, tissue-inflammatory macrophages, to M2, wound healing macrophages; however, they can also be associated with the initiation of a foreign body reaction.[52−55] Data shown in this paper demonstrate the anti-inflammatory effect of the hydrogels and M2 polarization of the macrophages in the presence of NPs; therefore, the observed isolated MGCs were also associated with the M2 phenotype. However, further experiments should be carried out to fully understand the role of these MGCs in tissue repair processes. The prolonged anti-inflammatory effect of the hybrid hydrogels could be useful for the treatment of pro-inflammatory pathologies. Burch et al.[56] and Yen et al.[23] reported the anti-inflammatory activity of different Fmoc-dipeptides bearing aromatic amino acids, as the one tested in this work, both in vivo and in vitro, respectively. Moreover, their self-healing properties anticipate their employment as injectable hydrogels in the target area. It is well known that tissue regeneration is a complex phenomenon involving severe inflammation, oxidative stress, and bacterial infections. In particular, the incorporation of natural substances having antibacterial properties could be of interest,[57,58] and even showing both effects, anti-inflammatory and antibacterial, as in the case of essential oils that contain, e.g., eugenol and carvacrol.[59] The antibacterial properties of Fmoc-FFpY hydrogels have been previously reported[9] that make the Fmoc-FFpY/NPs hydrogels suitable to prevent bacterial infection on the surgery site or in the context of chronic wounds. Moreover, they could also be used for cell encapsulation in the context of tissue engineering and regeneration medicine.[60,61]

4. CONCLUSIONS

Supramolecular hybrid hydrogels were formed by the electrostatic interaction of a water-soluble phosphorylated tripeptide, Fmoc-FFpY, with cationic polymer nanoparticles, poly(HKT-*co*-VI) NPs exhibiting a high-density peptide fibers network around the polymer NPs. The peptide self-assembly structure adopted two different fiber morphologies, nontwisted fibers attributed to β-sheet conformations and twisted fibers assigned to α-helix arrangements, the predominant structure according to CD. The rheological properties of the hybrid hydrogel showed an 8-fold increase of G', from ∼11 to ∼84 Pa, as the Fmoc-FFpY concentration increased from 2.5 to 5 mg mL^{-1}. These hydrogels are injectable as they showed shear thinning behavior and self-healing properties with a complete recovery of their viscoelastic properties after being subjected to high (1000%) and low (1%) strains at short times. When in contact with PBS at 37 °C, Fmoc-FFpY and poly(HKT-*co*-VI) NPs are released with the same profile, a fast release for 2 days followed by a plateau. A good biocompatibility of the hydrogels was obtained toward human fibroblasts and murine macrophages. Finally, Fmoc-FFpY/poly(HKT-*co*-VI) NPs hydrogels have the ability to prevent the polarization of macrophages to pro-inflammatory phenotype and decrease the NO production to basal values (∼33%) proving their excellent anti-inflammatory property. These hybrid peptide/polymer NPs hydrogels are the ideal candidate for the minimally invasive treatment of inflammatory diseases.

ASSOCIATED CONTENT

Supporting Information

The Supporting Information is available free of charge at https://pubs.acs.org/doi/10.1021/acsami.1c22993.

Inverted tube tests of hydrogels over the time (Figure S1), cryo-TEM micrographs (Figure S2), dynamic step strain amplitude tests (Figure S3), hydrogels stability in DMEM (Figure S4) and in contact with FBH and RAW cells (Figure S5), FBH and RAW cell viability in contact with Fmoc-FFpY (Figure S6), FBH cell adhesion (Figure S7), nitric oxide released by lipopolysaccharide-stimulated (LPS) RAW cells in contact with Fmoc-FFpY (Figure S8), nitric oxide released by lipopolysaccharide-stimulated (LPS) RAW cells in contact with different concentrations of Fmoc-FFpY (Figure S9), and nitric oxide released by lipopolysaccharide-stimulated (LPS) RAW cells in contact with aliquots extracted from Fmoc-FFpY/poly(HKT-*co*-VI) hydrogels in contact with cell culture medium (Figure S10) (PDF)

AUTHOR INFORMATION

Corresponding Author

Miryam Criado-Gonzalez − *Instituto de Ciencia y Tecnología de Polímeros (ICTP-CSIC), 28006 Madrid, Spain;* orcid.org/0000-0002-5502-892X; Email: mcriado@ictp.csic.es

Authors

Eva Espinosa-Cano − *Instituto de Ciencia y Tecnología de Polímeros (ICTP-CSIC), 28006 Madrid, Spain; CIBER-BBN, 28029 Madrid, Spain*

Luis Rojo − *Instituto de Ciencia y Tecnología de Polímeros (ICTP-CSIC), 28006 Madrid, Spain; CIBER-BBN, 28029 Madrid, Spain*

Fouzia Boulmedais − *Université de Strasbourg, CNRS, Institut Charles Sadron (UPR 22), 67034 Strasbourg, France;* orcid.org/0000-0002-4934-9276

María Rosa Aguilar − *Instituto de Ciencia y Tecnología de Polímeros (ICTP-CSIC), 28006 Madrid, Spain; CIBER-BBN, 28029 Madrid, Spain*

Rebeca Hernández − *Instituto de Ciencia y Tecnología de Polímeros (ICTP-CSIC), 28006 Madrid, Spain;* orcid.org/0000-0001-7332-0134

Complete contact information is available at: https://pubs.acs.org/10.1021/acsami.1c22993

Author Contributions

‖M.C.-G. and E.E.-C. contributed equally. The manuscript was written through contributions of all authors. All authors have given approval to the final version of the manuscript. M.C.-G. contributed to conceptualization, methodology, investigation, formal analysis, data curation, writing—review & editing, supervision, and project administration. E.E.-C. contributed to methodology and investigation. L.R. performed investigation. F.B. carried out data curation, supervision, and writing—review & editing. M.R.A. contributed to conceptualization and supervision. R.H. performed supervision, writing—review & editing, and project administration.

Funding

Financial support from Spanish Research Council (CSIC) and French Research Council (CNRS) for the project PICS (International Emerging Actions) 2018 HYDROPRINT is

gratefully acknowledged. The authors also acknowledge funding from CIBER-BBN, Spanish Ministry of Science, Innovation and Universities (MAT2017-83014-C2-2-P and MAT2017-84277-R), and the training program for Academic Staff, grant number FPU15/06109, of the Spanish Ministry of Education Culture and Sport

Notes

The authors declare no competing financial interest.

■ ACKNOWLEDGMENTS

Dr. Rafael Nuñez from CIB-CSIC is gratefully acknowledged for TEM and Cryo-TEM measurements. M.R.A. and L.R. are members of the Nanomedicine CSIC HUB (ref 202180E048).

■ REFERENCES

(1) Lee, A. L. Z.; Voo, Z. X.; Chin, W.; Ono, R. J.; Yang, C.; Gao, S.; Hedrick, J. L.; Yang, Y. Y. Injectable Coacervate Hydrogel for Delivery of Anticancer Drug-Loaded Nanoparticles in vivo. *ACS Appl. Mater. Interfaces* **2018**, *10*, 13274−13282.

(2) Rodon Fores, J.; Criado-Gonzalez, M.; Chaumont, A.; Carvalho, A.; Blanck, C.; Schmutz, M.; Boulmedais, F.; Schaaf, P.; Jierry, L. Autonomous Growth of a Spatially Localized Supramolecular Hydrogel with Autocatalytic Ability. *Angew. Chem., Int. Ed.* **2020**, *59*, 14558−14563.

(3) Yuk, H.; Lu, B.; Lin, S.; Qu, K.; Xu, J.; Luo, J.; Zhao, X. 3D Printing of Conducting Polymers. *Nat. Commun.* **2020**, *11*, No. 1604.

(4) Ren, P.; Li, J.; Zhao, L.; Wang, A.; Wang, M.; Li, J.; Jian, H.; Li, X.; Yan, X.; Bai, S. Dipeptide Self-assembled Hydrogels with Shear-Thinning and Instantaneous Self-healing Properties Determined by Peptide Sequences. *ACS Appl. Mater. Interfaces* **2020**, *12*, 21433−21440.

(5) Mondal, S.; Das, S.; Nandi, A. K. A Review on Recent Advances in Polymer and Peptide Hydrogels. *Soft Matter* **2020**, *16*, 1404−1454.

(6) Radvar, E.; Azevedo, H. S. Supramolecular Peptide/Polymer Hybrid Hydrogels for Biomedical Applications. *Macromol. Biosci.* **2019**, *19*, No. 1800221.

(7) Conte, M. P.; Sahoo, J. K.; Abul-Haija, Y. M.; Lau, K. H. A.; Ulijn, R. V. Biocatalytic Self-Assembly on Magnetic Nanoparticles. *ACS Appl. Mater. Interfaces* **2018**, *10*, 3069−3075.

(8) Ruan, L.; Chen, W.; Wang, R.; Lu, J.; Zink, J. I. Magnetically Stimulated Drug Release Using Nanoparticles Capped by Self-Assembling Peptides. *ACS Appl. Mater. Interfaces* **2019**, *11*, 43835−43842.

(9) Criado-Gonzalez, M.; Iqbal, M. H.; Carvalho, A.; Schmutz, M.; Jierry, L.; Schaaf, P.; Boulmedais, F. Surface Triggered Self-Assembly of Fmoc-Tripeptide as an Antibacterial Coating. *Front. Bioeng. Biotechnol.* **2020**, *8*, No. 938.

(10) Lim, J. H.; Park, J.; Ahn, J. H.; Jin, H. J.; Hong, S.; Park, T. H. A Peptide Receptor-Based Bioelectronic Nose for the Real-Time Determination of Seafood Quality. *Biosens. Bioelectron.* **2013**, *39*, 244−249.

(11) Wang, Y.; Versluis, F.; Oldenhof, S.; Lakshminarayanan, V.; Zhang, K.; Wang, Y.; Wang, J.; Eelkema, R.; Guo, X.; van Esch, J. H. Directed Nanoscale Self-Assembly of Low Molecular Weight Hydrogelators Using Catalytic Nanoparticles. *Adv. Mater.* **2018**, *30*, No. 1707408.

(12) Eming, S. A.; Krieg, T.; Davidson, J. M. Inflammation in Wound Repair: Molecular and Cellular Mechanisms. *J. Invest. Dermatol.* **2007**, *127*, 514−525.

(13) Kester, M.; Karpa, K. D.; Vrana, K. E. 10 - Inflammatory Disorders. In *Elsevier's Integrated Review Pharmacology*, 2nd ed.; Kester, M.; Karpa, K. D.; Vrana, K. E., Eds.; W.B. Saunders: Philadelphia, 2012; pp 161−172.

(14) Raziyeva, K.; Kim, Y.; Zharkinbekov, Z.; Kassymbek, K.; Jimi, S.; Saparov, A. Immunology of Acute and Chronic Wound Healing. *Biomolecules* **2021**, *11*, 700.

(15) Anderson, K.; Hamm, R. L. Factors That Impair Wound Healing. *J. Am. Coll. Clin. Wound Spec.* **2012**, *4*, 84−91.

(16) Xu, Z.; Liang, B.; Tian, J.; Wu, J. Anti-Inflammation Biomaterial Platforms for Chronic Wound Healing. *Biomater. Sci.* **2021**, *9*, 4388−4409.

(17) Espinosa-Cano, E.; Aguilar, M. R.; Vázquez, B.; San Román, J. Chapter 7 - Inflammation-Responsive Polymers. In *Smart Polymers and their Applications*, 2nd ed.; Aguilar, M. R.; San Román, J., Eds.; Woodhead Publishing, 2019; pp 219−254.

(18) Espinosa-Cano, E.; Aguilar, M. R.; Portilla, Y.; Barber, D. F.; San Román, J. Anti-Inflammatory Polymeric Nanoparticles Based on Ketoprofen and Dexamethasone. *Pharmaceutics* **2020**, *12*, No. 723.

(19) Nienhaus, K.; Wang, H.; Nienhaus, G. U. Nanoparticles for Biomedical Applications: Exploring and Exploiting Molecular Interactions at the Nano-Bio Interface. *Mater. Today Adv.* **2020**, *5*, No. 100036.

(20) Zhang, Y.; Gu, H.; Yang, Z.; Xu, B. Supramolecular Hydrogels Respond to Ligand−Receptor Interaction. *J. Am. Chem. Soc.* **2003**, *125*, 13680−13681.

(21) Castelletto, V.; Moulton, C. M.; Cheng, G.; Hamley, I. W.; Hicks, M. R.; Rodger, A.; López-Pérez, D. E.; Revilla-López, G.; Alemán, C. Self-Assembly of Fmoc-Tetrapeptides Based on the RGDS Cell Adhesion Motif. *Soft Matter* **2011**, *7*, 11405−11415.

(22) Debnath, S.; Shome, A.; Das, D.; Das, P. K. Hydrogelation Through Self-Assembly of Fmoc-Peptide Functionalized Cationic Amphiphiles: Potent Antibacterial Agent. *J. Phys. Chem. B* **2010**, *114*, 4407−4415.

(23) Yen, C.-T.; Hwang, T.-L.; Wu, Y.-C.; Hsieh, P.-W. Design and Synthesis of New N-(fluorenyl-9-methoxycarbonyl) (Fmoc)-Dipeptides as Anti-Inflammatory Agents. *Eur. J. Med. Chem.* **2009**, *44*, 1933−1940.

(24) Ji, W.; Yuan, C.; Chakraborty, P.; Gilead, S.; Yan, X.; Gazit, E. Stoichiometry-Controlled Secondary Structure Transition of Amyloid-Derived Supramolecular Dipeptide co-Assemblies. *Commun. Chem.* **2019**, *2*, No. 65.

(25) Ji, W.; Yuan, C.; Zilberzwige-Tal, S.; Xing, R.; Chakraborty, P.; Tao, K.; Gilead, S.; Yan, X.; Gazit, E. Metal-Ion Modulated Structural Transformation of Amyloid-Like Dipeptide Supramolecular Self-Assembly. *ACS Nano* **2019**, *13*, 7300−7309.

(26) Jayawarna, V.; Ali, M.; Jowitt, T. A.; Miller, A. F.; Saiani, A.; Gough, J. E.; Ulijn, R. V. Nanostructured Hydrogels for Three-Dimensional Cell Culture Through Self-Assembly of Fluorenylmethoxycarbonyl−Dipeptides. *Adv. Mater.* **2006**, *18*, 611−614.

(27) Yang, Z.; Xu, B. Using Enzymes to Control Molecular Hydrogelation. *Adv. Mater.* **2006**, *18*, 3043−3046.

(28) Vigier-Carrière, C.; Garnier, T.; Wagner, D.; Lavalle, P.; Rabineau, M.; Hemmerlé, J.; Senger, B.; Schaaf, P.; Boulmedais, F.; Jierry, L. Bioactive Seed Layer for Surface-Confined Self-Assembly of Peptides. *Angew. Chem., Int. Ed.* **2015**, *54*, 10198−10201.

(29) Criado-Gonzalez, M.; Fores, J. R.; Carvalho, A.; Blanck, C.; Schmutz, M.; Kocgozlu, L.; Schaaf, P.; Jierry, L.; Boulmedais, F. Phase Separation in Supramolecular Hydrogels Based on Peptide Self-Assembly from Enzyme-Coated Nanoparticles. *Langmuir* **2019**, *35*, 10838−10845.

(30) Criado-Gonzalez, M.; Loftin, B.; Rodon Fores, J.; Vautier, D.; Kocgozlu, L.; Jierry, L.; Schaaf, P.; Boulmedais, F.; Harth, E. Enzyme Assisted Peptide Self-Assemblies Trigger Cell Adhesion in High Density Oxime Based Host Gels. *J. Mater. Chem. B* **2020**, *8*, 4419−4427.

(31) Criado-Gonzalez, M.; Wagner, D.; Rodon Fores, J.; Blanck, C.; Schmutz, M.; Chaumont, A.; Rabineau, M.; Schlenoff, J. B.; Fleith, G.; Combet, J.; Schaaf, P.; Jierry, L.; Boulmedais, F. Supramolecular Hydrogel Induced by Electrostatic Interactions between Polycation and Phosphorylated-Fmoc-Tripeptide. *Chem. Mater.* **2020**, *32*, 1946−1956.

(32) De Caris, M. G.; Grieco, M.; Maggi, E.; Francioso, A.; Armeli, F.; Mosca, L.; Pinto, A.; D'Erme, M.; Mancini, P.; Businaro, R. Blueberry Counteracts BV-2 Microglia Morphological and Functional Switch after LPS Challenge. *Nutrients* **2020**, *12*, 1830.

https://doi.org/10.1021/acsami.1c22993
ACS Appl. Mater. Interfaces 2022, 14, 10068−10080

(33) Criado-Gonzalez, M.; Wagner, D.; Iqbal, M. H.; Ontani, A.; Carvalho, A.; Schmutz, M.; Schlenoff, J. B.; Schaaf, P.; Jierry, L.; Boulmedais, F. Supramolecular Tripeptide Self-Assembly Initiated at the Surface of Coacervates by Polyelectrolyte Exchange. *J. Colloid Interface Sci.* **2021**, *588*, 580−588.
(34) Tang, C.; Ulijn, R. V.; Saiani, A. Effect of Glycine Substitution on Fmoc−Diphenylalanine Self-Assembly and Gelation Properties. *Langmuir* **2011**, *27*, 14438−14449.
(35) Smith, A. M.; Williams, R. J.; Tang, C.; Coppo, P.; Collins, R. F.; Turner, M. L.; Saiani, A.; Ulijn, R. V. Fmoc-Diphenylalanine Self Assembles to a Hydrogel via a Novel Architecture Based on $\pi-\pi$ Interlocked β-Sheets. *Adv. Mater.* **2008**, *20*, 37−41.
(36) Li, X.; Zhou, G.-J.; Chu, G.-H.; Lin, X.-F.; Wang, J.-L.; Shen, K.; Yin, J. Fabrication of Size-Controllable mPEG-Decorated Microparticles Conjugating Optically Active Ketoprofen Based on Self-Assembly of Amphiphilic Random Copolymers. *J. Appl. Polym. Sci.* **2013**, *127*, 3242−3248.
(37) Socrates, G. *Infrared and Raman Characteristic Group Frequencies: Tables and Charts*; John Wiley and Sons Ltd: United Kingdom, 2001.
(38) Fleming, S.; Frederix, P. W. J. M.; Ramos Sasselli, I.; Hunt, N. T.; Ulijn, R. V.; Tuttle, T. Assessing the Utility of Infrared Spectroscopy as a Structural Diagnostic Tool for β-Sheets in Self-Assembling Aromatic Peptide Amphiphiles. *Langmuir* **2013**, *29*, 9510−9515.
(39) Mu, X.; Eckes, K. M.; Nguyen, M. M.; Suggs, L. J.; Ren, P. Experimental and Computational Studies Reveal an Alternative Supramolecular Structure for Fmoc-Dipeptide Self-Assembly. *Biomacromolecules* **2012**, *13*, 3562−3571.
(40) Rajkumar, B. J. M.; Ramakrishnan, V. Vibrational Spectroscopic Study of Dl-Methionine Dihydrogen Phosphate. *Spectrochim. Acta, Part A* **2001**, *57*, 247−254.
(41) Venyaminov, S. Y.; Kalnin, N. N. Quantitative IR Spectrophotometry of Peptide Compounds in Water (H2O) Solutions. I. Spectral Parameters of Amino Acid Residue Absorption Bands. *Biopolymers* **1990**, *30*, 1243−1257.
(42) Xing, R.; Yuan, C.; Li, S.; Song, J.; Li, J.; Yan, X. Charge-Induced Secondary Structure Transformation of Amyloid-Derived Dipeptide Assemblies from β-Sheet to α-Helix. *Angew. Chem., Int. Ed.* **2018**, *57*, 1537−1542.
(43) Ryan, D. M.; Anderson, S. B.; Senguen, F. T.; Youngman, R. E.; Nilsson, B. L. Self-Assembly and Hydrogelation Promoted by F5-Phenylalanine. *Soft Matter* **2010**, *6*, 475−479.
(44) Krysmann, M. J.; Castelletto, V.; Kelarakis, A.; Hamley, I. W.; Hule, R. A.; Pochan, D. J. Self-Assembly and Hydrogelation of an Amyloid Peptide Fragment. *Biochemistry* **2008**, *47*, 4597−4605.
(45) Wang, F.; Gnewou, O.; Wang, S.; Osinski, T.; Zuo, X.; Egelman, E. H.; Conticello, V. P. Deterministic Chaos in the Self-Assembly of β Sheet Nanotubes from an Amphipathic Oligopeptide. *Matter* **2021**, *4*, 3217−3231.
(46) Saunders, L.; Ma, P. X. Self-Healing Supramolecular Hydrogels for Tissue Engineering Applications. *Macromol. Biosci.* **2019**, *19*, No. 1800313.
(47) Ding, X.; Gao, J.; Wang, Z.; Awada, H.; Wang, Y. A Shear-Thinning Hydrogel that Extends In Vivo Bioactivity of FGF2. *Biomaterials* **2016**, *111*, 80−89.
(48) Xing, R.; Li, S.; Zhang, N.; Shen, G.; Möhwald, H.; Yan, X. Self-Assembled Injectable Peptide Hydrogels Capable of Triggering Antitumor Immune Response. *Biomacromolecules* **2017**, *18*, 3514−3523.
(49) Du, E. Y.; Ziaee, F.; Wang, L.; Nordon, R. E.; Thordarson, P. The Correlations between Structure, Rheology, and Cell Growth in Peptide-Based Multicomponent Hydrogels. *Polym. J.* **2020**, *52*, 947−957.
(50) Anderson, J. M.; Andukuri, A.; Lim, D. J.; Jun, H.-W. Modulating the Gelation Properties of Self-Assembling Peptide Amphiphiles. *ACS Nano* **2009**, *3*, 3447−3454.
(51) Abalymov, A. A.; Santos, C. A. B.; Van der Meeren, L.; Van de Walle, D.; Dewettinck, K.; Parakhonskiy, B. V.; Skirtach, A. G. Nanofibrillar Hydrogels by Temperature Driven Self-Assembly: New Structures for Cell Growth and Their Biological and Medical Implications. *Adv. Mater. Interfaces* **2021**, *8*, No. 2002202.
(52) Islam, S.; Hassan, F.; Tumurkhuu, G.; Dagvadorj, J.; Koide, N.; Naiki, Y.; Mori, I.; Yoshida, T.; Yokochi, T. Bacterial Lipopolysaccharide Induces Osteoclast Formation in RAW 264.7 Macrophage Cells. *Biochem. Biophys. Res. Commun.* **2007**, *360*, 346−351.
(53) Miron, R. J.; Bosshardt, D. D. Multinucleated Giant Cells: Good Guys or Bad Guys? *Tissue Eng., Part B* **2018**, *24*, 53−65.
(54) Barbeck, M.; Booms, P.; Unger, R.; Hoffmann, V.; Sader, R.; Kirkpatrick, C. J.; Ghanaati, S. Multinucleated Giant Cells in the Implant Bed of Bone Substitutes are Foreign Body Giant Cells—New Insights into the Material-mediated Healing Process. *J. Biomed. Mater. Res., Part A* **2017**, *105*, 1105−1111.
(55) Brooks, P. J.; Glogauer, M.; McCulloch, C. A. An Overview of the Derivation and Function of Multinucleated Giant Cells and Their Role in Pathologic Processes. *Am. J. Pathol.* **2019**, *189*, 1145−1158.
(56) Burch, R. M.; Weitzberg, M.; Blok, N.; Muhlhauser, R.; Martin, D.; Farmer, S. G.; Bator, J. M.; Connor, J. R.; Ko, C.; Kuhn, W.; McMillan, B. A.; Raynor, M.; Shearer, B. G.; Tiffany, C.; Wilkins, D. E. N-(Fluorenyl-9-Methoxycarbonyl) Amino Acids, a Class of Antiinflammatory Agents With a different Mechanism of Action. *Proc. Natl. Acad. Sci. U.S.A.* **1991**, *88*, 355−359.
(57) Douglas, T. E. L.; Dziadek, M.; Schietse, J.; Boone, M.; Declercq, H. A.; Coenye, T.; Vanhoorne, V.; Vervaet, C.; Balcaen, L.; Buchweitz, M.; Vanhaecke, F.; Van Assche, F.; Cholewa-Kowalska, K.; Skirtach, A. G. Pectin-Bioactive Glass Self-Gelling, Injectable Composites with High Antibacterial Activity. *Carbohydr. Polym.* **2019**, *205*, 427−436.
(58) He, W.; Wang, Z.; Hou, C.; Huang, X.; Yi, B.; Yang, Y.; Zheng, W.; Zhao, X.; Yao, X. Mucus-Inspired Supramolecular Adhesives with Oil-Regulated Molecular Configurations and Long-Lasting Antibacterial Properties. *ACS Appl. Mater. Interfaces* **2020**, *12*, 16877−16886.
(59) Alkattan, R.; Rojo, L.; Deb, S. Antimicrobials in Dentistry. *Appl. Sci.* **2021**, *11*, 3279.
(60) Zhou, M.; Smith, A. M.; Das, A. K.; Hodson, N. W.; Collins, R. F.; Ulijn, R. V.; Gough, J. E. Self-Assembled Peptide-Based Hydrogels as Scaffolds for Anchorage-Dependent Cells. *Biomaterials* **2009**, *30*, 2523−2530.
(61) Wang, Y.-L.; Lin, S.-P.; Nelli, S. R.; Zhan, F.-K.; Cheng, H.; Lai, T.-S.; Yeh, M.-Y.; Lin, H.-C.; Hung, S.-C. Self-Assembled Peptide-Based Hydrogels as Scaffolds for Proliferation and Multi-Differentiation of Mesenchymal Stem Cells. *Macromol. Biosci.* **2017**, *17*, No. 1600192.

https://doi.org/10.1021/acsami.1c22993
ACS Appl. Mater. Interfaces 2022, 14, 10068−10080